Penman, D. E., Turner, S. K., Sexton, P. F., Norris, R. D., Dickson, A. J., Boulila, S., Ridgwell, A., Zeebe, R. E., Zachos, J. C., Cameron, A., Westerhold, T., & Röhl, U. (2016). An abyssal carbonate compensation depth overshoot in the aftermath of the Palaeocene-Eocene Thermal Maximum. *Nature Geoscience*, *9*(8), 575-580. https://doi.org/10.1038/ngeo2757

A carbonate compensation depth overshoot in the aftermath of the Paleocene-Eocene Thermal Maximum

Donald E. Penman
Sandra Kirtland Turner
Philip Sexton
Richard Norris
Alexander J. Dickson
Slah Boulila
Andy Ridgwell
Richard E. Zeebe
James Zachos
Adele Cameron
Thomas Westerhold
Ursula Röhl
IODP Expedition 342 Scientists

During the Paleocene-Eocene Thermal Maximum (PETM, ~56Ma), thousands of petagrams of carbon were released into the atmosphere and oceans in just a few thousand years (kyr), followed by gradual sequestration over ~200 kyr. Theory and carbon cycle models predict that if silicate weathering is one of the key negative feedbacks responsible for the removal of this carbon, a period of calcium carbonate oversaturation (relative to pre-event levels) should have occurred during the event's recovery. This could be reflected in the marine geological record as an over-deepening of the calcite compensation depth (CCD). However, despite previous evidence for enhanced calcium carbonate accumulation at shallow depths following the PETM, no direct observations of this hypothesized CCD over-deepening have yet been made. Here we present evidence from two new North Atlantic sections that test this hypothesis. Consistent with existing records, we find higher calcite accumulation during the PETM recovery phase compared to pre-event accumulation at a mid-abyssal site (U1409), demonstrating intensified post-PETM

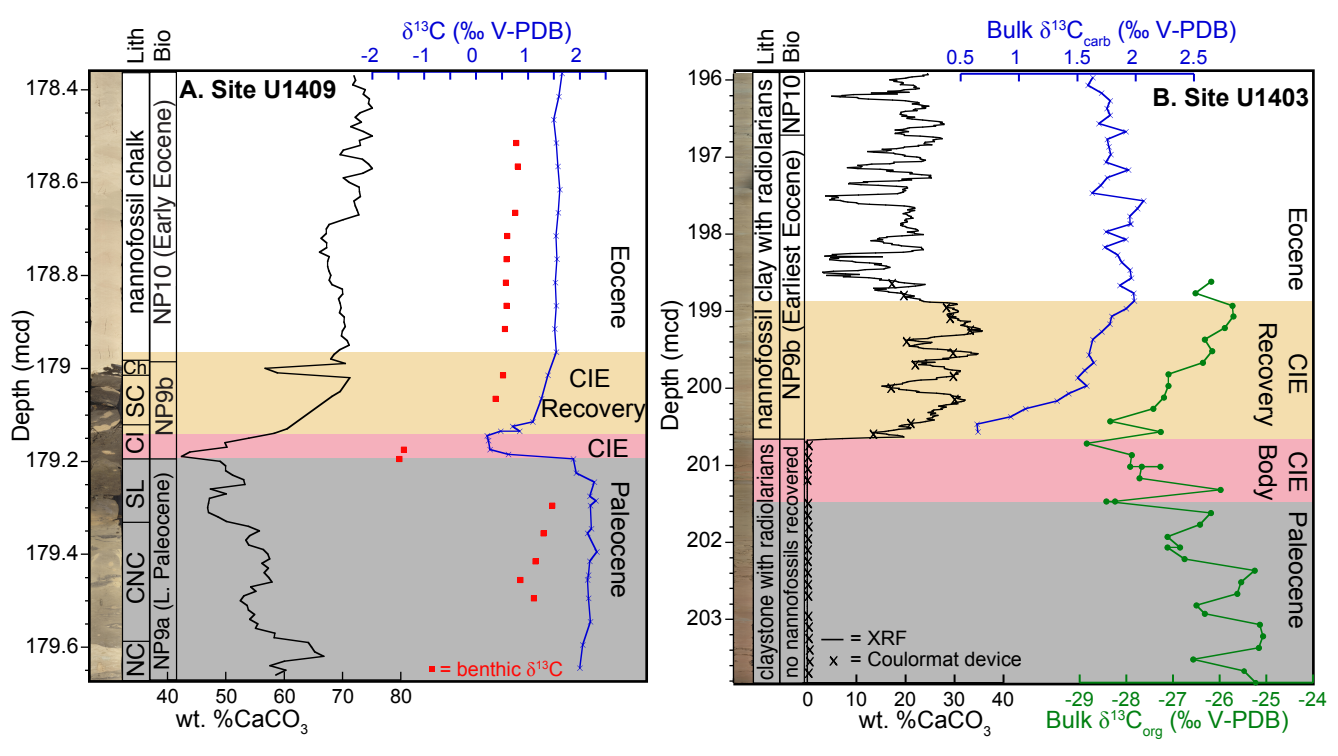
A. Site U1409
B. Site U1403
Lith
Bio
δ13C (‰ V-PDB)
Bulk δ13Ccarb (‰ V-PDB)
Depth (mcd)
nannofossil chalk
NP10 (Early Eocene)
Ch
SC
Cl
SL
CNC
NC
NP9b
NP9a (L. Paleocene)
Eocene
CIE Recovery
CIE
Paleocene
= benthic δ13C
wt. %CaCO3
nannofossil clay with radiolarians
NP9b (Earliest Eocene)
NP10
CIE Body
claystone with radiolarians
no nannofossils recovered
= XRF
= Coulormat device
Bulk δ13Corg (‰ V-PDB)

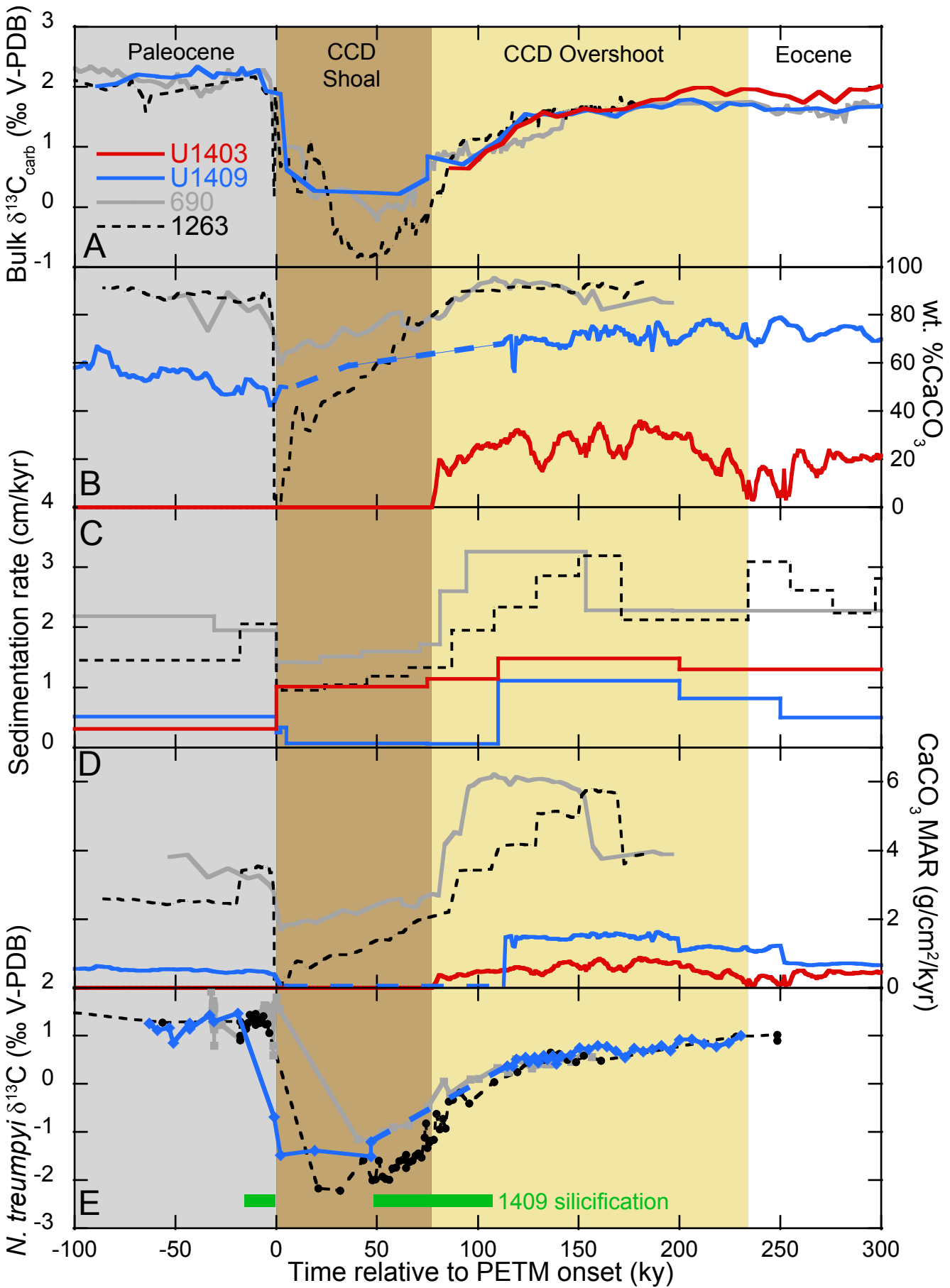
Paleocene
CCD Shoal
CCD Overshoot
Eocene
U1403
U1409
690
1263
A
B
C
D
E
Bulk δ13Ccarb (‰ V-PDB)
wt. %CaCO3
Sedimentation rate (cm/kyr)
CaCO3 MAR (g/cm2/kyr)
N. treumpyi δ13C (‰ V-PDB)
1409 silicification
Time relative to PETM onset (ky)

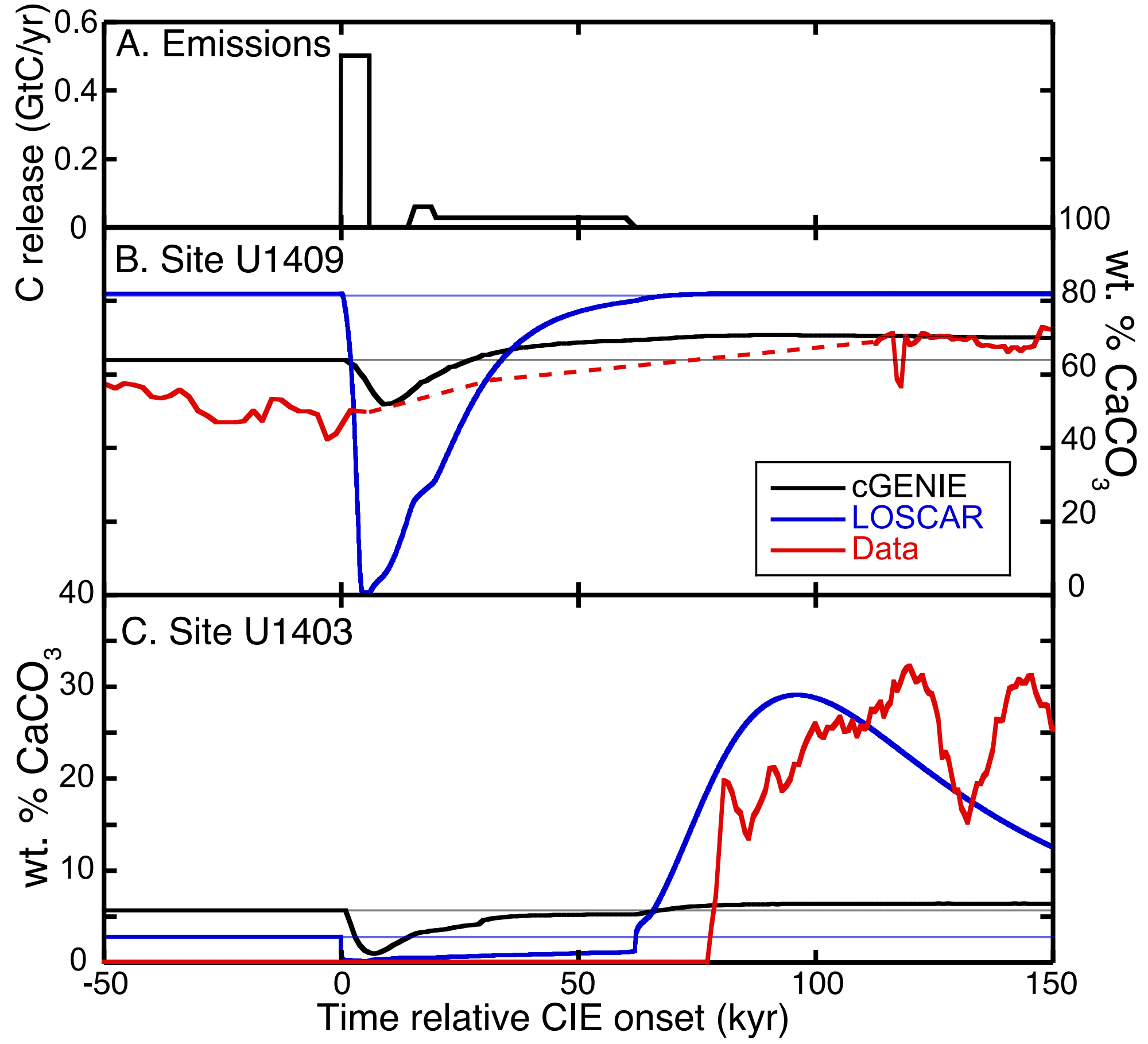
A. Emissions
B. Site U1409
C. Site U1403
C release (GtC/yr)
0.6
0.4
0.2
0
wt. % CaCO3
100
80
60
40
20
0
40
30
20
10
0
cGENIE
LOSCAR
Data
-50
0
50
100
150
Time relative CIE onset (kyr)

calcite preservation above the CCD. However, at a second, deeper (lower abyssal) site (U1403) that comprises calcite-barren clay prior to the PETM, we observe a transition to calcite-rich during the PETM recovery, providing the first observational evidence of the posited post-PETM CCD over-deepening. We also find an ~70 kyr lag between the PETM onset and CCD overshoot that is best explained in our Earth system model experiments by prolonged low-level PETM carbon emissions following a large initial carbon release. Our findings indicate that PETM carbon sequestration was accomplished by both globally enhanced calcite burial above the CCD and by an over-deepening of the CCD (at least in the North Atlantic), advancing our understanding of how the Earth system recovers from major carbon cycle perturbations.

The Paleocene-Eocene Thermal Maximum (PETM; ~56 Ma) represents one of the largest and most abrupt greenhouse warming events in Earth history. Marine and terrestrial records document a global >2.5‰ negative carbon isotope excursion (CIE)[1-3] coincident with global mean surface ocean warming of >4°C[4] and geochemical and sedimentological evidence for ocean acidification[5,6]. Collectively, these lines of evidence suggest a rapid (10^3-10^4 years) and massive (~3,000-10,000 PgC) release of ^{13}C-depleted carbon into the ocean-atmosphere system[7-9]. The PETM thus offers the opportunity to examine the response and recovery of the global carbon cycle and seawater carbonate chemistry to an ancient CO_2 release similar in magnitude to ongoing anthropogenic fossil fuel combustion[10].

Current understanding of long-term carbon cycle processes suggests that large-scale carbon injection into the ocean-atmosphere should induce a two-phase response in

ocean carbonate saturation. Initially, rapid invasion of CO_2 into the ocean lowers pH and carbonate saturation state (Ω) in tandem[6,11,12], resulting in dissolution of both newly deposited and pre-existing carbonate sediments[5]. The result is a dramatic reduction in $CaCO_3$ burial in marine sediments globally and, in places, evidence for a shoaling of the calcite compensation depth (CCD, the depth below which no calcium carbonate, in the form of calcite, is preserved).[5,13,14].

A second phase of carbonate saturation and burial response arises from elevated atmospheric pCO_2 and increased global temperatures that are thought to drive an increase in the rate of terrestrial carbonate and silicate rock chemical weathering[15,16], which can be generalized:

$$CaCO_3 + CO_2 + H_2O \rightarrow Ca^{2+} + 2HCO_3^- \quad (1)$$

$$CaSiO_3 + 2CO_2 + 3H_2O \rightarrow Ca^{2+} + 2HCO_3^- + H_4SiO_4 \quad (2)$$

Accelerating these reactions increases the delivery of Ca^{2+} (and thus total alkalinity) and dissolved inorganic carbon (DIC) to the oceans, elevating Ω. An intensification of continental weathering during the PETM is supported by a pronounced increase in the $^{187}Os/^{188}Os$ of seawater[17,18] and an increase in kaolinite in marine sediments[19]. However, although the silicate weathering rate responds quickly to increased temperature/CO_2, the rate of CO_2 drawdown from global weathering (~ 0.1 PgC/yr[11]) is small in comparison to estimates of initial carbon release (thousands of PgC)[7-9], meaning that this feedback should take $>10^4$ years to gradually overcome the undersaturation associated with the initial acidification phase[20-22]. On longer timescales ($>10^5$ years)[22], this increased weathering-derived flux of TA and DIC to the oceans must be balanced by carbonate production and burial to balance the ocean's alkalinity budget:

$$Ca^{2+} + 2HCO_3^- \rightarrow CaCO_3 + CO_2 + H_2O \quad (3)$$

The long-term balance of carbonate weathering with carbonate burial has no permanent effect on the ocean's TA or DIC budgets (Equation 1 is simply the reverse of Equation 3). However, the long-term balance of silicate weathering (Equation 2) with carbonate burial (Equation 3) gives rise to a net consumption of CO_2 that is buried as $CaCO_3$ sediment – the long-term fate of carbon released during the PETM.

The assumption that net CO_2 consumption (Equation 2+3) is responsive to a perturbation in climate forms the basis of a proposed long-term negative (stabilizing) feedback on climate, hypothesized to have been important in maintaining a habitable climate throughout Earth history[15,16] and specifically during the PETM recovery[20]. One way in which global carbonate burial could respond to changing weathering flux is through fluctuations of the global sea-floor area of carbonate-free sediments (i.e the CCD). In other words: during the initial acidification phase, carbonate undersaturation leads to a reduced $CaCO_3$ sink and a short-term shoaling of the CCD, whereas on longer timescales (>10^5 years), faster weathering rates lead to carbonate oversaturation and increased carbonate burial, which might be reflected in an over-deepening of the CCD[10,20,23]. The interval of excess (compared to pre-PETM) $CaCO_3$ burial primarily reflects the removal of carbon released at the onset of the PETM by enhanced silicate weathering, together with the quantity of $CaCO_3$ dissolved during the initial carbonate undersaturation phase and additional terrestrial weathering of carbonate rocks under warmer temperatures (both of which will be some function of CO_2 release). The characteristics of any post-PETM CCD overshoot hence potentially hold key information

regarding the magnitude of carbon release and the processes involved in the recovery from an abrupt carbon cycle perturbation.

A carbonate burial overshoot is a predicted consequence of the silicate weathering feedback. Indeed, the existence of a CCD over-deepening is predicted by several carbon cycle model simulations of the PETM that include such a feedback[9,20]. Yet no records exist from deep sites below the pre-PETM CCD with which to detect possible CCD over-deepening. Deep-sea sedimentary records from above the CCD (Southern Ocean Site 690 [24-27] at ~1900m paleodepth and South Atlantic Sites 1263[5,26,27] at ~1500m paleodepth and 1266[5,28] at ~2500m paleodepth) show increases in $CaCO_3$ content and accumulation rate during and after the PETM recovery[25-27]. These records are consistent with weathering feedbacks prompting increased carbonate burial during the PETM recovery. These supra-CCD records are important constraints because the long-term requirement to balance the elevated weathering flux only requires carbonate burial to increase globally (not necessarily buried at deeper depths), and it is theoretically possible to accommodate such elevated global carbonate burial without substantial deepening of the CCD[29]. Nonetheless, some models[9,10,20] predict that a testable facet of the recovery process from massive carbon cycle perturbation involves an over-deepening of the CCD, and the location of these sites above the pre-PETM CCD means that they cannot directly test for this predicted CCD over-deepening. Direct observational evidence sites deep enough to test for a post-PETM CCD overshoot has thus far remained elusive.

Here we present lithology, $CaCO_3$ content, and carbon isotope ($\delta^{13}C$) records from recently recovered sediment cores in the North Atlantic (IODP Sites U1403, PETM paleodepth ~4374m and U1409, paleodepth ~2913m[30]) that provide important constraints

on the evolution of the CCD through the PETM, including the first evidence for CCD over-deepening during the PETM recovery. To explore the broader implications of these records for PETM carbon emissions scenarios, we present new carbon release experiments using two carbon cycle models – LOSCAR[9,31] and cGENIE[32,33] and discuss uncertainties in the representation of geological carbon cycling in current models.

At Site U1409, the PETM CIE occurs in an interval of variously silicified sediments (siliceous claystones, siliceous limestones and cherts) at 178.9-179.2 mcd (Figure 1A), contrasting with the nannofossil chalk that characterizes much of the Paleogene at this site[30]. Although likely somewhat condensed, the $\delta^{13}C_{carb}$ record bears the typical[27] PETM CIE pattern of an abrupt decrease (here of ~2‰) followed by a plateau of low values and then gradual recovery (Fig. 1). Bulk $\delta^{13}C_{carb}$ over the PETM CIE interval sampled a heterogeneous mixture of lithology (clay, carbonate-rich burrows within that clay, and siliceous sediments), with all three lithologies revealing significantly lower $\delta^{13}C$ within the CIE than pre-event values. The integrity of the bulk $\delta^{13}C_{carb}$ record is also supported by the close structural similarity between it and the equivalent bulk $\delta^{13}C_{carb}$ records from the Southern Ocean and Walvis Ridge (Fig. 1, 2A). The Site U1409 $\delta^{13}C$ record from benthic foraminifera is discontinuous owing to silicification accross the onset and initial recovery, but minimum values within the CIE show a large (~3‰) excursion, similar to that seen in benthic records from the Southern Ocean[34] and South Atlantic[35]. Below the CIE, carbonate content is between 60-70 wt%, decreases to a minimum of ~40 wt% at the CIE onset, and rebounds to ~70% following the CIE. This pattern is similar to other pelagic PETM sections[14] and implies that the local CCD was always deeper than the paleodepth of Site U1409, while the decrease in carbonate during

the PETM can be interpreted as a transient decrease in the calcite saturation state, Ω, consistent with shoaling of the CCD. The absence of near-0 wt% $CaCO_3$ sediment at Site U1409 contrasts with records from the South Atlantic Ocean[5] where cores even shallower than U1409 are barren of carbonate within the CIE. Although this observation could imply that CCD shoaling in the North Atlantic was less dramatic than that in the South Atlantic, hiatuses, bioturbation by burrowing, or incomplete recovery of this silicified interval could have obscured or resulted in the loss of the interval containing the lowest wt% $CaCO_3$ values. Regardless, carbonate content and accumulation rate at Site U1409 were higher during the PETM recovery than before the event, similar to other sites at mid-ocean depths or shallower[5,24-26,28], thus providing support for elevated saturation states and increased carbonate burial above the CCD during the recovery phase.

Lower abyssal Site U1403 features a prominent transition (over ~5 cm) from carbonate-poor (<0.5 wt%) claystone in the Upper Paleocene (extending from the P-E boundary to at least ~61 Ma[30]) to carbonate-bearing (~20-30 wt%) nannofossil claystone in the lower Eocene (Figure 1B). This carbonate-rich interval contains calcareous nannofossils of zone NP9B, including PETM excursion taxa *Discoaster araneus* and *Rhomboaster* spp[30]. Bulk $\delta^{13}C_{org}$ reveals a negative CIE between 200.7 and 201.5 mcd that is superimposed on comparatively high amplitude orbital timescale variability in the late Paleocene. The $\delta^{13}C_{carb}$ record necessarily begins at the onset of carbonate sedimentation with low values of ~0.6‰, followed by a gradual 1.4‰ increase over the next ~1.6 m, parallel to the recovery in $\delta^{13}C_{org}$. Given the simultaneous trends to higher values in both $\delta^{13}C_{carb}$ and $\delta^{13}C_{org}$ within zone NP9B, this $\delta^{13}C$ increase can be unambiguously assigned to the PETM CIE recovery. The magnitude of the $\delta^{13}C_{carb}$

increase (1.4‰) is close to the full amplitude of the PETM CIE recovery observed in bulk carbonates globally[27] and at Site U1409 (Figure 2A), so we confidently assign the onset of carbonate sedimentation at Site U1403 to early in the PETM recovery phase.

We construct age models by correlating the $\delta^{13}C_{carb}$ records to a compilation of bulk and fine-fraction $\delta^{13}C_{carb}$ on an orbitally calibrated age model[27] (Figure 2A and 2C). This age model, based on several PETM sites, produces a shorter duration of the PETM CIE than extraterrestrial ^{3}He-based estimates,[24,28] so durations here may represent minima. On this timescale, carbonate sedimentation begins at Site U1403 ~70kyr after the PETM onset and is followed by a period of elevated (20-40) wt% $CaCO_3$ that persists for a further ~150kyr. Fluctuations between 5 and 25 wt% $CaCO_3$ continue throughout the lower Eocene. Although the CIE onset at Site U1403 as defined by the somewhat noisy $\delta^{13}C_{org}$ record introduces some uncertainty around the placement of the P-E boundary, this does not affect the relative timing of the initial appearance of carbonate at this lower abyssal site, which is unambiguously assigned to the PETM recovery interval based on $\delta^{13}C_{carb}$ and the occurrence of PETM excursion-interval calcareous nannofossils.

The pattern of carbonate sedimentation at Site U1403 (carbonate-barren in the Paleocene with carbonate appearing during the PETM recovery) has not previously been observed in sediments spanning the PETM. The absence of carbonate in the Upper Paleocene and into the earliest Eocene indicates the CCD lay shallower than Site U1403 before the PETM and through the CIE onset and body. The onset of carbonate sedimentation ~70kyr after the PETM onset indicates that the CCD over-deepened to below the ~4400 m lower abyssal paleo-water depth of Site U1403 during the early phase

of PETM recovery – direct evidence for a post-PETM CCD overshoot. The ~150kyr period of elevated carbonate deposition at Site U1403 represents the main phase of the CCD over-deepening, and is coeval with enhanced carbonate accumulation and preservation at shallower paleodepths documented here at Site U1409 and elsewhere[5,25,26,28] (Figure 2D). These observations strongly implicate elevated whole-ocean saturation state as the cause of enhanced carbonate burial at all water depths and from the North Atlantic to the Southern Ocean.

To explore the implications of a CCD overshoot and its timing, and the CCD over-deepening at U1403 in particular, we tested a variety of PETM carbon emissions scenarios using the models LOSCAR and cGENIE. Rather than carry out an extensive sweep of all combinations of plausible size and duration of carbon release, our emissions scenarios are based on ref. [9], characterized by an initial C input ($\delta^{13}C$ = -50‰) of 3000 PgC over 5 kyr, followed by 1480 PgC over 50 kyr, and originally developed to best match records of carbonate dissolution (particularly in the South Atlantic[5]). However, we explored a number of variations on this basic emissions trajectory (Figs. S4-S15) such as doubling the total mass with half the isotopic composition ($\delta^{13}C$ = -25‰). In order to isolate the response of carbonate burial dynamics from circulation effects that might diverge in the two models, we ran cGENIE with radiative forcing (and thus ocean circulation) fixed, and for direct comparison with cGENIE (Figure 3) we omitted the prescribed circulation changes of ref. 9 in LOSCAR. We tracked the evolution of global sedimentary wt% $CaCO_3$ preserved, and simulated the expected marine sediment record in modeled ‘cores’ at North Atlantic depths approximating Sites U1409 and U1403.

The configurations of both LOSCAR and cGENIE models used here include a CO_2-dependent silicate weathering feedback (see methods). Both models simulate a global CCD and wt% $CaCO_3$ overshoot which occurs between 20 and 45 kyr after the onset of carbon emissions and peaks between 65 and 97 kyr after the onset, depending on the emissions schedule and model (Figure 3 and Figure S3)[9,20]. The carbonate overshoot begins earlier when the carbon pulse occurs over a shorter interval of time (Figures S6, S12). The long delay (~70kyr) in the onset of carbonate sedimentation at Site U1403 that we infer from our age model is hence difficult to reconcile with only a short "spike" of carbon released at the onset of the PETM. Rather, the delay is better explained by a sustained release of carbon lasting many tens of kyr after an initial spike (Figure 3, S1), consistent with the conclusions of refs. [9] and [6]. Such sustained carbon release might arise as a feedback response to initial warming[36,37] or represent prolonged North Atlantic volcanism. Our experiments also demonstrate that the timing of the overshoot is not particularly sensitive to the mass of carbon released – doubling the mass of carbon results in < 2 kyr delay in overshoot timing (e.g. Figure S4 vs. Figure S5).

While both models generate a whole-ocean carbonate burial overshoot during the recovery interval, the spatial distribution of $CaCO_3$ content in sediments shows differences both between the models and in comparison to Sites U1403 and U1409 (Figure 3). Because LOSCAR has much coarser spatial resolution (e.g. it represents the deep Atlantic as a single box), regional patterns need to be interpreted with greater caution. Nevertheless, LOSCAR generates a deep (4500m) $\%CaCO_3$ overshoot comparable to that seen at Site U1403, but in shallow sediments (3000m) generates a larger $\%CaCO_3$ decrease (to near-zero) and smaller overshoot than seen at Site U1409. In

contrast, cGENIE closely matches the Site U1409 record, but at 5000m, sediments overshoot their pre-event %$CaCO_3$ levels by only ~1%, in conflict with the Site U1403 record. It appears that in response to enhanced weathering-driven elevated saturation states, LOSCAR accommodates greater global carbonate burial with higher %$CaCO_3$ in deep sediments (an over-deepening of the CCD), whereas cGENIE accommodates greater global carbonate burial predominantly within and above the lysocline. Observational evidence (in the form of new and previous carbonate accumulation rate records) suggest that in the real world (at least in the case of the PETM), both of these processes may operate.

The differences between the models' predictions for the locus of intensified carbonate burial result from of how the models represent sedimentary processes. In cGENIE, the respiration of organic carbon in sediments reduces porewater saturation state and dissolves $CaCO_3$ even in shallow sediments well above the carbonate saturation horizon. Because of this, those shallow sediments have greater potential to accommodate an increase in $CaCO_3$ content in response to higher bottom water saturation state such as that seen in the aftermath of the PETM. cGENIE thus balances enhanced weathering flux via elevated carbonate burial mostly in shallow sediments (within and above the lysocline)[29]. Conversely, %$CaCO_3$ in sediments above the lysocline in LOSCAR is set by the ratio of clay to $CaCO_3$ in the sediment rain (81% $CaCO_3$ in the present configuration)[31], so when saturation state increases those shallow sediments cannot accommodate higher $CaCO_3$ contents (they are already at a maximum). Hence, LOSCAR balances an increase in weathering flux via enhanced carbonate burial within the lysocline and below the (pre-event) CCD.

A notable aspect of the Site U1403 carbonate record is that following the main phase of the CCD over-deepening featuring the highest carbonate contents, wt% $CaCO_3$ does not return to 0% (its pre-event level) before the next major hyperthermal (ETM-2, ~2Myr later[30]) (Fig. 1, 2). Hence, the North Atlantic CCD did not return to its pre-PETM state. Two possible explanations exist for this observation. First, negative feedbacks on carbonate undersaturation could have been very slow to re-establish equilibrium. This is unlikely, given that all other records of environmental and carbon-cycle perturbation during the PETM (such as temperature[4], pH[38], and the CIE[27]) recovered in hundreds of thousands of years, not millions. Second, the carbon cycle might have transitioned to a new equilibrium state featuring a deeper CCD. Several mechanisms may help explain a deeper post-PETM equilibrium CCD in the North Atlantic. First, the PETM CCD evolution may have been superimposed on a long-term (multi-million year) global CCD deepening trend[39-42]. Increasing pCO_2 on multi-million year timescales across the Late Paleocene-Early Eocene from greater volcanic CO_2 release or an imbalance between terrestrial C_{org} oxidation and marine C_{org} burial could have strengthened weathering rates, thus increasing seawater carbonate saturation and driving a gradual CCD deepening from ~58 to ~52Ma, independently of the PETM[39]. Indeed, LOSCAR simulations of carbon release superimposed on gradual long-term CCD deepening (Figure S2) agree well with observations from Site U1403, including the persistence of the overshoot.

A second possibility is that changing ocean circulation or regional carbonate export across the PETM affected the regional North Atlantic CCD (i.e. the observed CCD over-deepening was not necessarily global). Weakened North Atlantic-sourced overturning during the acidification phase followed by strengthened overturning during

the oversaturation phase could have produced the initial large CCD shoal documented at Walvis Ridge[5] (South Atlantic) and the later CCD over-deepening at Site U1403 (North Atlantic). If such circulation changes persisted for several Myr, they could have produced a persistently deeper post-PETM North Atlantic CCD. Spatial benthic $\delta^{13}C$ gradients can shed light on circulation changes[34], because the accumulation of respired C_{org} reduces the $\delta^{13}C$ of deep water DIC as it ages. Owing to its location in the lower abyss, Site U1403 is unfortunately nearly barren of benthic foraminifera throughout the PETM and its recovery. However, Site U1409 benthic $\delta^{13}C$ values overlap with those of South Atlantic[35] and Southern Ocean[34] during intervals immediately prior to the PETM and during the later stages of the recovery, including the time interval (>110kyr after the event) during which Site U1403 documents a CCD overshoot (Figure 2). Benthic gradients between the South and North Atlantic therefore do not show any evidence for large-scale changes in Atlantic overturning circulation during the PETM recovery that could have contributed to a localized CCD over-deepening.

It is also possible that the CCD over-deepening was influenced by other carbon sequestration processes operating during the PETM recovery that removed carbon from the ocean/atmosphere and increased seawater pH and saturation state (in a sense, the opposite of the PETM acidification phase), and hence influence the CCD. In particular, studies have suggested that the pace of the CIE recovery, which is complete within ~150kyr[24,28], is too rapid to be explained by enhanced weathering and carbonate burial alone. Instead, the preferential removal of ^{12}C via enhanced burial of organic carbon (C_{org}) has been proposed to explain the CIE recovery timing[43]. This is consistent with evidence of increased marine productivity during the PETM from elevated biogenic

barium accumulation rates[44,45] and coccolith Sr/Ca[46]. Our model experiments focus on the long-term inorganic carbon cycle and silicate weathering and hence cannot exclude a role for enhanced organic carbon burial.

In summary: our finding of a post-PETM CCD overshoot in the North Atlantic Ocean constitutes the first evidence for post-PETM variations in carbonate burial from sediments deeper than the pre-PETM CCD. It thus represents an important constraint on the vertical extent of the CCD's response to carbon release during the PETM and consequently, the processes responsible for restoring the carbon cycle to steady state. It is tempting to use this constraint to directly calculate the mass of carbon released during the PETM because the excess carbonate burial should scale with the mass of carbon released. However, we recognize that one site does not fully constrain the global extent of the overshoot, nor its absolute magnitude. Further constraints on the CCD over-deepening from even deeper water depths and additional ocean basins are therefore an essential target for future scientific drilling. Additionally, uncertainty in the parameterization and strength of the silicate weathering feedback (Figure S2)[47] as well as the potential influences of initial carbon cycle conditions, circulation changes, C_{org} burial, and changing clay flux preclude explicit calculation of the total carbon release[10]. Indeed, the differing responses of the two different global carbon cycle models we have tested against the observations underscore the lack of consensus on how the marine carbonate carbon sink responds in detail (and particularly in the depth distribution of $CaCO_3$ burial) to perturbation. Multiple combinations of mass and rate of carbon release, weathering feedback strength, and C_{org} burial are consistent with the new observations described here. Our findings nevertheless provide an important constraint on how carbon was

sequestered in the aftermath of the PETM, an event that continues to guide our understanding of Earth system processes and feedbacks during large-scale carbon cycle perturbations.

Author Contributions: DP, SKT, PS, RN, and SB conceived the study and participated in IODP Expedition 342 that recovered and described the sediments used here. DP generated carbonate stable isotope analyses in the lab of JZ, and AD generated organic carbon stable isotope and Coulormat %$CaCO_3$ analyses. XRF records were generated by SKT at Scripps, and AC, PS, TW, and UR at MARUM. DP and SKT performed the carbon cycle modeling with guidance from RZ and AR. DP drafted the manuscript, SKT contributed cGENIE modeling text, and all authors edited the manuscript.

Acknowledgements: We thank the scientists and crew of IODP Expedition 342 and the Bremen Core Repository. The comments of two anonymous reviewers greatly improved the manuscript. This work was supported by NSF OCE-1220615 to JZ and RZ.

METHODS

Geochemical analyses

During IODP Expedition 342, drilling operations penetrated the P-E boundary at Sites U1403 (39°56.5997N, 51°48.1998W, 4946m depth) and U1409 (41°17.7501N, 49°13.9996W, 3502m depth). Shipboard investigation described lithology, identified the approximate positions of the P-E boundary by nannofossil biostratigraphy, and provided coarse-resolution records of wt% $CaCO_3$. The surface of core archive halves spanning the

PETM were scanned at 1-2 cm-resolution at the MARUM – Center for Marine Environmental Sciences, University of Bremen and at Scripps Institution of Oceanography using Avaatech X-ray fluorescence (XRF) core scanners. Estimates of the total abundance of calcium (Ca) and iron (Fe) were obtained by scanning cores at an energy level of 10kV, current of 500 uA, count time of 20 sec, and measurement area of 10 x 12 mm. Estimated wt% $CaCO_3$ records were generated by regressing shipboard wt% $CaCO_3$ measurements[30] against the natural logarithm of XRF-derived Ca/Fe ratios. For stable isotope analyses, samples were collected at ~5cm resolution from Site U1409 and 10cm resolution from Site U1403, freeze dried, homogenized with mortar and pestle, and analyzed for $\delta^{13}C_{carb}$ on a ThermoFisher MAT 253 stable isotope mass spectrometer coupled to a Kiel IV carbonate device using standard dual-inlet techniques. In addition, samples from Site U1409 were washed and sieved, and specimens of the benthic foraminifera *Nuttalides truempyi* were picked from the 150-200 and 212-300μm size fraction. Where possible, 3-8 of these specimens from each sample were run using the $\delta^{13}C_{carb}$ methods described above. For $\delta^{13}C_{org}$ analysis of Site U1403, homogenized sample powders were de-carbonated in 1M HCL and washed in de-ionized water. $\delta^{13}C_{org}$ was measured using a Thermo-Finnegan MAT 253 mass spectrometer coupled to a Thermo Scientific 2000 HT elemental analyzer via a Conflo IV interface optimized for the measurement of samples with low organic carbon abundances. Analytical reproducibility was monitored using analyses of IAEA CH-6 sucrose and was < ±0.1‰ (1 S.D). All $\delta^{13}C$ data are expressed relative to V-PDB. Additional Site U1403 wt. % $CaCO_3$ was measured using a Strohlein Coulormat.

Carbon cycle modeling

LOSCAR is a numerically-efficient geochemical box model of the marine carbon cycle with realistic interaction with sediments, capable of multi-million year simulations of carbon cycle processes including CCD depth. All runs use Paleogene LOSCAR setup[31]. cGENIE is an intermediate-complexity Earth system model including a 3-D dynamic ocean model with biogeochemical cycling of key elements and isotopes and a spatially resolved sediment model capable of generating virtual sediment cores – synthetic stacks of deep-sea sediments[32,33,48]. We use the late Paleocene/early Eocene configuration of ref. [12]. For this study, we evaluate virtual sediment core results from a depth transect in the North Atlantic ranging from 5000-3000 m water depth and at locations corresponding to Expedition 342 sites.

Both models include carbonate and silicate weathering feedbacks. In LOSCAR, weathering is parameterized as $F_w = F_{eq} * ([CO_2]_{atm} / [CO_2]_{eq})^{Nsi}$, where F_{eq} and $[CO_2]_{eq}$ are equilibrium weathering flux and atmospheric pCO_2 at which volcanic carbon emissions are perfectly balanced by silicate weathering and carbonate burial[31]. N_{Si} sets the strength of the silicate weathering feedback (default $N_{Si} = 0.2$). We implement the same formulation for a CO_2-dependent carbonate and silicate weathering feedback in cGENIE using a model for terrestrial rock weathering[49]. Following ref. [50], we assume carbonate weathering proportional to the square root of $[CO_2]_{atm} / [CO_2]_{eq}$ and silicate weathering proportional to $[CO_2]_{atm} / [CO_2]_{eq}$ raised to the power of 0.3. We assume a 50:50 split between carbonate and silicate weathering in order to match total carbonate burial, and balance silicate weathering with volcanic outgassing. We utilize the cGENIE and LOSCAR models in this study in order to qualitatively demonstrate what

mechanisms are consistent with the new data, not in an attempt to reconstruct exactly a PETM scenario.

FIGURE CAPTIONS

Figure 1: Lithology and $\delta^{13}C$ over the PETM at Sites U1409 (top) and U1403 (bottom) plotted against composite depth (mcd). Each panel shows core photo (Site U1403 vertically compressed), lithologic description, calcareous nannofossil biostratigraphy, wt. %$CaCO_3$ estimated by XRF (black line), and bulk $\delta^{13}C_{carb}$ (blue line). Bulk $\delta^{13}C_{org}$ (green line) and wt. % $CaCO_3$ measured with a Coulormat device (black X's) are also shown for Site U1403, and benthic foraminifer *Nuttalides truempyi* $\delta^{13}C$ (red squares) is shown for Site U1409. Depth intervals representing the Paleocene, CIE, Recovery, and post-PETM based on $\delta^{13}C$ stratigraphy are highlighted with grey, red, orange, and white shaded bars, respectively. PETM phases nomenclature from ref. 32.

Figure 2: A: Bulk $\delta^{13}C_{carb}$ records from Sites 690[25], 1263[27], U1403, and U1409 plotted on the age model used in this study. B: Weight %$CaCO_3$ of Sites U1403 and U1409 (this study), 690[25], and 1263[5]. C: Linear sedimentation rates used in age models constructed by this study for Sites U1403 and U1409, and Sites 690 and 1263 from Röhl, et al. [27] D: Carbonate mass accumulation rate calculated from dry bulk density, sedimentation rates (C), wt. % $CaCO_3$ (B). E: Comparison of benthic foraminifer $\delta^{13}C$ from South Atlantic Site 1263,[35] Southern Ocean Site 690,[34] and U1409 demonstrating small and constant North-South aging gradient during the CCD overshoot. Green bars indicate silicified intervals at Site U1409 which precluded measurement of benthic foraminifers. In (B), (D) and (E), the silicified interval of U1409 is marked with a dashed line to reflect potential

hiatuses or incomplete recovery which may have resulted in an incomplete %$CaCO_3$ record (see text).

Figure 3: Comparison of LOSCAR and cGENIE C release experiments using the Emissions scenario of ref. 9 with radiative forcing (and thus circulation) fixed in cGENIE, and no circulation changes in LOSCAR. Top panel: Emissions scenario. Middle panel: modeled 3000m sediment core-top %$CaCO_3$ compared with Site U1409 %CaCO3 record. Bottom panel: modeled 4500m (LOSCAR) and 5000m (cGENIE) sediment core-top %$CaCO_3$ compared with Site U1403 %CaCO3 record. In middle and bottom panels, thin, opaque traces mark pre-event %$CaCO_3$ for cGENIE and LOSCAR.

Figure S1: LOSCAR modeling of the CCD overshoot. A: Carbon emissions forcing for spike (0.6PgC/yr for 5kyr) and spike + leak (0.11PgC/yr for an additional 65kyr) scenarios. B: Evolution of the modeled Atlantic CCD in response to spike and spike + leak scenarios. Without a sustained leak, the CCD overshoots within ~15kyr, in contrast to the Site U1403 record C: Large sensitivity of the CCD overshoot magnitude, timing, and duration to the strength of the weathering feedback, which is poorly constrained. Weathering flux is parameterized in LOSCAR as $F_w = F_{eq} * ([CO_2]_{atm} / [CO_2]_{eq})^{Nsi}$, where F_{eq} and $[CO_2]_{eq}$ are equilibrium weathering flux and atmospheric pCO_2 at which volcanic carbon emissions are perfectly balanced by silicate weathering and carbonate burial [31]. N_{Si} is a free parameter in the model which sets the strength of the silicate weathering feedback (default $N_{Si} = 0.2$). All scenarios are spike only.

Figure S2: Atlantic CCD evolution of a single 6 kyr 3000 GtC pulse superimposed on a long-term CCD deepening trend forced by increasing volcanic carbon flux by 15% over 3Ma.

Figure S3: Comparison of LOSCAR and cGENIE C release experiments using double the emissions scenario of Zeebe et al., 2009. LOSCAR includes the circulation switch of Zeebe et al., 2009, while cGENIE is run with radiative forcing (and thus circulation) fixed. Top panel: Emissions scenario. Middle panel: modeled 3000m sediment %$CaCO_3$ compared with Site U1409 %CaCO3 record. Bottom panel: modeled 4500m(LOSCAR) and 5000m (cGENIE) sediment %$CaCO_3$ compared with Site U1403 %CaCO3 record. Modeled cGENIE wt% $CaCO_3$ decreases appear to slightly precede emissions (Figs. 3 & S3) as a result of the effects of mixing, sediment rain input, and dissolution on carbonate age, which can thus deviate from current model time.

Figures S4-S9: cGENIE model output of various mass and timing of C release, with radiative forcing (and hence circulation) held constant (top panels) and radiative forcing responding to pCO_2 (bottom panel). Plotted are virtual sediment cores from 5000 and 3000m depth with %$CaCO_3$ and carbonate $\delta^{13}C$ plotted against sediment age, global mean sediment wt% $CaCO_3$, and C emissions forcing plotted against model time.

S4: Emissions scenario of Zeebe et al., 2009

S5: Double the emissions scenario of Zeebe et al., 2009 and input $\delta^{13}C$ = -25‰

S6: The total mass of Zeebe et al., 2009 injected in one 10 kyr pulse

S7: Double the total mass of Zeebe et al., 2009 injected in one 10kyr pulse

S8: The total mass of Zeebe et al., 2009 injected in one 20 kyr pulse

S9: Double the total mass of Zeebe et al., 2009 injected in one 20kyr pulse

Figures S10-S15: LOSCAR model output of various mass and timing of C release. Plotted are $\delta^{13}C$ of the surface Atlantic, atmospheric pCO_2, CCD depth of each ocean basin, and globally averaged, 3000m Atlantic, and 4500m Atlantic $\%CaCO_3$ versus model time.

S10: Emissions scenario of Zeebe et al., 2009

S11: Double the emissions scenario of Zeebe et al., 2009 and input $\delta^{13}C = 25‰$

S12: The total mass of Zeebe et al., 2009 injected in one 10 kyr pulse

S13: Double the total mass of Zeebe et al., 2009 injected in one 10kyr pulse

S14: The total mass of Zeebe et al., 2009 injected in one 20 kyr pulse

S15: Double the total mass of Zeebe et al., 2009 injected in one 20kyr pulse

Figure S16: Bulk carbonate and organic carbon isotope data and raw XRF intensity data from Site U1403 plotted against composite depth (mcd).

Figure S17: Bulk carbonate carbon isotope data and raw XRF intensity data from Site U1409 plotted against composite depth (mcd).

Table S1: Age model tie points for Sites U1403 and U1409, based on correlation of the bulk carbon isotope records at both sites to the compilation of ref. 32.

References

1 Koch, P. L., Zachos, J. C. & Gingerich, P. D. Correlation Between Isotope Records in Marine and Continental Carbon Reservoirs Near the Palaeocene Eocene Boundary. *Nature* **358**, 319-322 (1992).

2 Kennett, J. P. & Stott, L. D. Abrupt Deep-Sea Warming, Palaeoceanographic Changes and Benthic Extinctions At the End of the Palaeocene. *Nature* **353**, 225-229 (1991).

3 McInerney, F. A. & Wing, S. The Paleocene-Eocene Thermal Maximum: A Perturbation of Carbon Cycle, Climate, and Biosphere with Implications for the future. *Annual Review of Earth & Planetary Sciences* **39**, 489-516 (2011).

4 Dunkley-Jones, T. *et al.* Climate model and proxy data constraints on ocean warming across the Paleocene-Eocene Thermal Maximum. *Earth-Science Reviews* **125**, 123-145 (2013).

5 Zachos, J. C. *et al.* Rapid acidification of the ocean during the Paleocene-Eocene thermal maximum. *Science* **308**, 1611-1615 (2005).

6 Penman, D. E., Hönisch, B., Zeebe, R. E., Thomas, E. & Zachos, J. C. Rapid and sustained surface ocean acidification during the Paleocene‐Eocene Thermal Maximum. *Paleoceanography* (2014).

7 Dickens, G. R., Oneil, J. R., Rea, D. K. & Owen, R. M. Dissociation of Oceanic Methane Hydrate As a Cause of the Carbon Isotope Excursion At the End of the Paleocene. *Paleoceanography* **10**, 965-971 (1995).

8 Panchuk, K., Ridgwell, A. & Kump, L. R. Sedimentary response to Paleocene-Eocene Thermal Maximum carbon release: A model-data comparison. *Geology* **36**, 315-318 (2008).

9 Zeebe, R. E., Zachos, J. C. & Dickens, G. R. Carbon dioxide forcing alone insufficient to explain Palaeocene-Eocene Thermal Maximum warming. *Nature Geoscience* **2**, 576-580, doi:10.1038/ngeo578 (2009).

10 Zeebe, R. & Zachos, J. Long-term legacy of massive carbon input to the Earth system: Anthropocene vs. Eocene. *Philosophical Transactions of the Royal Society*, 1-22 (2012).

11 Hönisch, B. *et al.* The Geological Record of Ocean Acidification. *Science* **335**, 1058-1063 (2012).

12 Ridgwell, A. & Schmidt, D. N. Past Constraints on the vulnerability of marine calcifiers to massive carbon dioxide release. *Nature Geoscience* **3**, 196-200 (2010).

13 Sluijs, A., Zachos, J. C. & Zeebe, R. E. Constraints on hyperthermals. *Nature Geosci* **5**, 231-231 (2012).

14 Zeebe, R. E. & Zachos, J. C. Reversed deep-sea carbonate ion basin gradient during Paleocene-Eocene thermal maximum. *Paleoceanography* **22**, - (2007).

15 Walker, J. C. G., Hays, P. B. & Kasting, J. F. A Negative Feedback Mechanism for the Long-Term Stabilization of Earths Surface-Temperature. *J Geophys Res-Oc Atm* **86**, 9776-9782 (1981).

16 Berner, R. A., Lasaga, A. C. & Garrels, R. M. The carbonate-silicate geochemical cycle and its effects on atmospheric carbon dioxide over the past 100 million years. *American Journal of Science* **283**, 641-683 (1983).

17 Dickson, A. J. *et al.* Evidence for weathering and volcanism during the PETM from Arctic Ocean and Peri-Tethys osmium isotope records. *Palaeogeography Palaeoclimatology Palaeoecology* (in press).

18 Ravizza, G., Norris, R. N., Blusztajn, J. & Aubry, M. P. An osmium isotope excursion associated with the late Paleocene thermal maximum: Evidence of intensified chemical weathering. *Paleoceanography* **16**, 155-163 (2001).

19 Robert, C. & Kennett, J. P. Antarctic Subtropical Humid Episode At the Paleocene-Eocene Boundary - Clay-Mineral Evidence. *Geology* **22**, 211-214 (1994).
20 Dickens, G. R., Castillo, M. M. & Walker, J. C. G. A blast of gas in the latest Paleocene: Simulating first-order effects of massive dissociation of oceanic methane hydrate. *Geology* **25**, 259-262 (1997).
21 Goodwin, P. & Ridgwell, A. Ocean‐atmosphere partitioning of anthropogenic carbon dioxide on multimillennial timescales. *Global Biogeochemical Cycles* **24** (2010).
22 Lord, N., Ridgwell, A., Thorne, M. & Lunt, D. An impulse response function for the "long tail" of excess atmospheric CO2 in an Earth system model. *Global Biogeochemical Cycles* (2015).
23 Palike, H., Lyle, M., Nishi, H. & al., e. A Cenozoic record of the equatorial Pacific carbonate compensation depth. *Nature* **488**, 609-614 (2012).
24 Farley, K. A. & Eltgroth, S. F. An alternative age model for the Paleocene-Eocene thermal maximum using extraterrestrial He-3. *Earth and Planetary Science Letters* **208**, 135-148 (2003).
25 Kelly, D. C., Zachos, J. C., Bralower, T. J. & Schellenberg, S. A. Enhanced terrestrial weathering/runoff and surface ocean carbonate production during the recovery stages of the Paleocene-Eocene thermal maximum. *Paleoceanography* **20**, - (2005).
26 Kelly, D. C., Nielsen, T. M. J., McCarren, H. K., Zachos, J. C. & Rohl, U. Spatiotemporal patterns of carbonate sedimentation in the South Atlantic: Implications for carbon cycling during the Paleocene-Eocene thermal maximum. *Palaeogeography Palaeoclimatology Palaeoecology* **293**, 30-40 (2010).
27 Röhl, U., Westerhold, T., Bralower, T. J. & Zachos, J. C. On the duration of the Paleocene-Eocene thermal maximum (PETM). *Geochemistry Geophysics Geosystems* **8**, - (2007).
28 Murphy, B. H., Farley, K. A. & Zachos, J. C. An extraterrestrial He-3-based timescale for the Paleocene-Eocene thermal maximum (PETM) from Walvis Ridge, IODP Site 1266. *Geochimica Et Cosmochimica Acta* **74**, 5098-5108 (2010).
29 Greene, S. *et al.* in *2014 AGU Fall Meeting Abstracts*. PP41C-1407.
30 Norris, R. *et al.* Paleogene Newfoundland sediment drifts. *Integrated Ocean Drilling Program: Preliminary Reports*, 1-263 (2012).
31 Zeebe, R. LOSCAR: Long-term ocean-atmosphere-sediment carbon cycle reservoir model v2. 0.4. *Geoscientific Model Development* **5**, 149-166 (2012).
32 Ridgwell, A. & Hargreaves, J. Regulation of atmospheric CO2 by deep‐sea sediments in an Earth system model. *Global Biogeochemical Cycles* **21** (2007).
33 Ridgwell, A. Interpreting transient carbonate compensation depth changes by marine sediment core modeling. *Paleoceanography* **22** (2007).
34 Nunes, F. & Norris, R. D. Abrupt reversal in ocean overturning during the Palaeocene/Eocene warm period. *Nature* **439**, 60-63 (2006).
35 McCarren, H., Thomas, E., Röhl, U. & Zachos, J. C. The Paleocene-Eocene Carbon Isotope Excursion: Insights from the benthic record (ODP Leg 208, Walvis Ridge). *Geophysics, Geosystems, Geochemistry* (2008).

36 Zeebe, R. E. What caused the long duration of the Paleocene‐Eocene Thermal Maximum? *Paleoceanography* **26**, 1-13 (2013).
37 Bowen, G. J. Up in smoke: A role for organic carbon feedbacks in Paleogene hyperthermals. *Global and Planetary Change* **109**, 18-29 (2013).
38 Penman, D. E., Hönisch, B., Zeebe, R. E., Thomas, E. & Zachos, J. C. Rapid and sustained surface ocean acidification during the Paleocene‐Eocene Thermal Maximum. *Paleoceanography* **29**, 357-369 (2014).
39 Komar, N., Zeebe, R. & Dickens, G. Understanding long‐term carbon cycle trends: The late Paleocene through the early Eocene. *Paleoceanography* **28**, 650-662 (2013).
40 Leon-Rodriguez, L. & Dickens, G. R. Constraints on ocean acidification associated with rapid and massive carbon injections: The early Paleogene record at ocean drilling program site 1215, equatorial Pacific Ocean. *Palaeogeography, Palaeoclimatology, Palaeoecology* **298**, 409-420 (2010).
41 Hancock, H. J., Dickens, G. R., Thomas, E. & Blake, K. L. Reappraisal of early Paleogene CCD curves: foraminiferal assemblages and stable carbon isotopes across the carbonate facies of Perth Abyssal Plain. *International Journal of Earth Sciences* **96**, 925-946 (2007).
42 Slotnick, B. *et al.* Early Paleogene variations in the calcite compensation depth: new constraints using old boreholes across Ninetyeast Ridge in the Indian Ocean. *Climate of the Past Discussions* **10**, 3163-3221 (2014).
43 Bowen, G. J. & Zachos, J. C. Rapid carbon sequestration at the termination of the Palaeocene-Eocene Thermal Maximum. *Nature Geoscience* **3**, 866-869 (2010).
44 Bains, S., Norris, R. D., Corfield, R. M. & Faul, K. L. Termination of global warmth at the Palaeocene/Eocene boundary through productivity feedback. *Nature* **407**, 171-174 (2000).
45 Ma, Z. *et al.* Carbon sequestration during the Palaeocene-Eocene Thermal Maximum by an efficient biological pump. *Nature Geoscience* (2014).
46 Stoll, H. M. & Bains, S. Coccolith Sr/Ca records of productivity during the Paleocene-Eocene thermal maximum from the Weddell Sea. *Paleoceanography* **18** (2003).
47 Uchikawa, J. & Zeebe, R. E. Influence of terrestrial weathering on ocean acidification and the next glacial inception. *Geophysical Research Letters* **35** (2008).
48 Ridgwell, A. Application of sediment core modelling to interpreting the glacial-interglacial record of Southern Ocean silica cycling. *Clim Past* **3**, 387-396 (2007).
49 Colbourn, G., Ridgwell, A. & Lenton, T. The Rock Geochemical Model (RokGeM) v0. 9. *Geoscientific Model Development* **6**, 1543-1573 (2013).
50 Walker, J. C. G. & Kasting, J. F. Effects of fuel and forest conservation on future levels of atmospheric carbon dioxide. *Palaeogeogr., Palaeoclimatol., Palaeoecol.* **97**, 151-189 (1992).